IEEE Access
Multidisciplinary | Rapid Review | Open Access Journal

Received July 11, 2018, accepted September 3, 2018, date of publication September 13, 2018, date of current version October 8, 2018.

Digital Object Identifier 10.1109/ACCESS.2018.2869702

Cellular Data Analytics for Detection and Discrimination of Body Movements

STEFANO SAVAZZI[1], (Member, IEEE), SANAZ KIANOUSH[1], (Member, IEEE), VITTORIO RAMPA[1], (Member, IEEE), AND UMBERTO SPAGNOLINI[2], (Senior Member, IEEE)

[1]Consiglio Nazionale delle Ricerche, Institute of Electronics, Computer and Telecommunication Engineering, 20133 Milano, Italy
[2]DEIB Department, Politecnico di Milano, 20133 Milano, Italy

Corresponding author: Stefano Savazzi (stefano.savazzi@ieiit.cnr.it)

ABSTRACT In this paper, we show the possibility of using the smartphone built-in cellular radio modem to track sudden changes in the environment around it, thus turning the cellphone into a radio–frequency (RF) virtual sensor. In particular, we demonstrate how to isolate anomalous RF patterns by applying time series modeling and analysis of downlink multi-cell radio signals. These RF anomalies may indicate a situation change, namely, a body or object(s), movement in the surrounding of the smart-phone. Unlike Wi-Fi and Bluetooth devices, that can be turned on and off according to the user demands, cellular radios are never really disconnected. Even in idle mode, they carry out continuous and autonomous measurements of the radio channel conditions, namely, the cellular signal quality (CSQ). This is performed in agreement with standardized cell reselection procedures. Body movements or scene changes in general in the surroundings of a cellular device are responsible for small CSQ fluctuations that can be isolated from normal network operations and classified accordingly. The validation of this unconventional RF sensing method is based on extensive measurement campaigns covering a period of one month, using up to four commercial off-the-shelf smartphones. As a practical application case study, we developed a real-time demonstrator that is able to detect body proximity events close to the device and discriminate other body-induced environmental changes in the surrounding of the smartphone. Usage of data analytics tools for passive sensing from cellular signals is a novel topic that shows great potential as paving the way to new applications and research opportunities.

INDEX TERMS Motion detection, wireless wide area networking, cellular signal quality, anomaly detection, bayesian classification, segmentation, data analytics, mobile phone-sensing, machine learning.

I. INTRODUCTION

Cellular radio devices represent an ideal platform for studying behaviour and interactions of people in real-life contexts. In fact, they are ubiquitous and unobtrusive, as users are not generally aware of their presence. Mobile devices are equipped with multiple wireless wide area networking (WWAN) air technologies *i.e.,* ranging from the GERAN radio access for 2G, UMTS terrestrial radio access (UTRA) for 3G, evolved UMTS terrestrial radio access (E-UTRA) for 4G (LTE, LTE-A and LTE-A Pro), up to the New Radio (NR) air interface for the forthcoming 5G networks. Unlike WiFi, Bluetooth and other local networking technologies, whose coverage over unlicensed bands is not always guaranteed and subject to interference, cellular networks are truly ubiquitous and rapidly evolving to support new functionalities, including device-to-device communication [1] as well as integration with Internet of Things (IoT) [2] and WLAN [3].

In this paper, we show how to turn any cellular (*i.e.,* WWAN-enabled) radio modem into a passive virtual detector of sudden changes in the environment around it. The use of cellular radios, besides enabling wide area networking and communication functions, is proposed here as a new paradigm for distributed stand-alone environmental sensing/detection systems that can be seamlessly integrated within existing phone-sensing platforms [4], [5], while enabling always-active operation. Sensing is herein based on the real-time analysis of the cellular signal quality (CSQ) indicators that measure the radio link propagation. Therefore, front-end processing tasks are independent of the specific device, sensor hardware and operating system. In addition, as previously mentioned, the availability of standardized

2169-3536 © 2018 IEEE. Translations and content mining are permitted for academic research only.
Personal use is also permitted, but republication/redistribution requires IEEE permission.
See http://www.ieee.org/publications_standards/publications/rights/index.html for more information.

multiple Radio Access Technologies (RATs) makes this new sensing capability independent of WWAN operators and available worldwide.

In the *idle mode* state, namely turned on, camped on a cell but not engaged in any sessions, every cellular device carries out continuous measurements of the radio channel conditions, looking for any chance to reselect from the camped cell to a new *better* one from the neighboring set. This is done to comply with the mobility procedures of WWAN standards and without any user intervention. The presence and/or the movement of objects in the surroundings of a fixed WWAN-enabled device result in a small change of the radio propagation conditions between the transmitter(s) *i.e.,* the cell site(s) or tower(s), and the receiver *i.e.,* the user equipment (UE), that measures the CSQ. Alterations in the environment surrounding the UE can thus be recognized in real-time by properly analyzing CSQ time series, and changes therein.

The purpose of the paper is to make an unique attempt towards the proposal and validation of data processing algorithms that enable the use of cellular radio signals for human-scale environmental sensing purposes. The research activities shown in this article are based upon the emerging paradigms of device-free radio sensing [6], [7] and radio vision [8]. However, while device-free human sensing [9], through-wall imaging [10] and localization [11] methods rely on a distributed wireless local area network (WLAN) of peer-to-peer radio nodes, the method proposed here depends on a cellular wide area network of UE terminals that communicate only exploiting a centralized set of base-stations with no local communication involved. The adoption of data analytics methods for cellular signals is a novel topic and it is introduced in Sect. II. Compared to other radio sources, processing of cellular data captured by the UE is more challenging. In fact, CSQ is subject to changing dynamics due to varying WWAN configurations and reselection from the camped cell to new ones. Stochastic modeling of such changes is considered in Sect. III while CSQ data analytics for detection and classification of changes around the smartphone are detailed in Sect. IV. The proposed tools are first validated in Sect. V based on extensive measurement campaigns using commercial off-the-shelf (COTS) smartphones, by comparing different methods for anomaly classification. Finally, in Sect. VI, we developed and deployed a real-time demonstrator platform where cellular signals are exploited for recognition and classification of environmental alterations, namely to discriminate body motions in close proximity to the device from other scene alterations *i.e.,* to detect if the smartphone is being picked up, manipulated or tampered with.

II. APPLYING DATA PROCESSING TO CELL SIGNALS

The human sensing by WLAN has been recently discussed from a communication perspective (see Guo *et al.* [12] and [13] in the Special Section: "Behavior Recognition Based on Wi-Fi CSI"). Unlike WLAN-based sensing methods, cellular signals captured by the UEs originate from cellular towers at distance in the order of several hundred meters

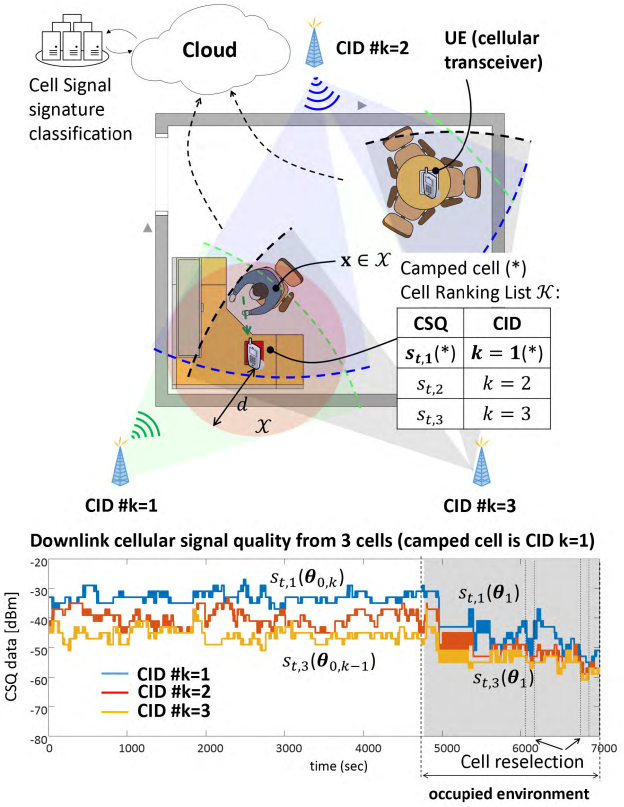

FIGURE 1. Example of changing CSQ dynamics due to network-driven and body occupancy events. The downlink CSQ is measured by one cell-phone for 3 UTRA high speed packet access (HSPA) enabled cells ($k = 1, 2, 3$). Data extraction is performed by using the AT + ECSQ command.

for urban areas, and up to some kilometers for rural ones. Moreover, these signals are subject to changing power levels and dynamics due to varying network configurations. In some cases, these perturbations may trigger the reselection from the camped cell to a *new* one (*cell reselection*). Typical WWANs are also characterized by a multiplicity of cellular towers each serving multiple cells to guarantee wide area coverage. Each cell is uniquely identified by a cell ID (CID) that indicates one or more antennas, serving frequency or RAT of the same cell tower. Cell reselection for the UE in idle mode can be triggered by many factors [14] as a consequence of time-varying changes of the network loading, as well as network configurations, cell power control or status, signal failures due to changes of the radio propagation scenario, UE mobility, in-hand manipulation or interference, just to cite a few.

According to the generic scenario of Fig. 1, the UEs are assumed to be in the idle mode state and to occupy fixed positions in the area of interest, namely the detection area, a room or an open environment. According to its RAT protocol, when camped on a cell, the UE must regularly check if there is a better cell according to the cell reselection criterion, and, if found, make a reselection towards this new cell. In order to support cell reselection, CSQ measurements must be performed and collected continuously by the UE to capture the characteristics of the radio channel of both currently

serving cell and neighboring ones *i.e.,* the members of the neighbor cell list. In the example of Fig. 1 at bottom, the CSQ data for 3 cells $s_{t,k}$ correspond to the time-varying camped ($k = 1$) and neighbor ($k = 2, 3$) cells at time t. These values may be retrieved from the UE, without no intervention of the network, by exploiting standard query commands (*i.e.,* AT commands) performed at the application layer through custom, or third-party apps, as shown in Sects. III-B and III-C. Sequential analytics for detection is applied here to the vector $\mathbf{s}_t = [s_{t,1}, s_{t,2}, s_{t,3}]$ that contains the joint CSQ measurements of the camped $s_{t,1}$ and the neighbor $s_{t,2}$, $s_{t,3}$ cells. As described in Sect. III, CSQ dynamics are governed by cell-specific RF propagation parameters in response to both *intrinsic* changes due to network operations and *extrinsic* alterations due to environment changes in the surroundings of the UE. Intrinsic changes are modelled here by parameters $\boldsymbol{\theta}_{0,k}$ that can be easily learned during an online training stage. A change in the environment inside the detection area $\mathcal{X}$ surrounding the cell-phone adds peculiar variations of the cellular signal levels that make such parameters to change into (unknown) $\boldsymbol{\theta}_1 \neq \boldsymbol{\theta}_{0,k}$.

III. CSQ AND MULTI-CELL RESELECTION MODELING

In this section, we develop a model for the dynamic evolution of the multi-cell RF signals from the UE perspective. Cell reselection is evaluated autonomously by each UE in idle mode using CSQ measurements obtained from a *cell ranking list* $\mathcal{K}$ and performed periodically by the terminal itself. Reselection from the serving cell to the new one causes abrupt changes of the observed CSQ dynamics. In most cases, reselection is not attributable to body movements but it can be due to many factors, mainly network-driven events. On the contrary, environmental changes caused by body/object movements are responsible of extra, but small, variations of the CSQ that, in many cases, affect multiple cells in the ranking list (Fig. 1), as being the result of the permanent, or temporary, alterations made in the surroundings of the UE. These changes can be both *additive* and *non-additive*. Moreover, depending on the cell status, CSQ changes might also trigger *new* reselections that add to those normally observed in idle mode.

A. MODELING OF DOWNLINK MULTI-CELL SIGNAL QUALITY

CSQ measurements are influenced by long- and short-term fading random effects that may be altered by environmental changes, and are thus modelled in this section as stochastic processes. Let $s_{t,k}$ be the CSQ measure at discrete time t captured by a UE from a cell identified by the CID k. The vector $\mathbf{s}_{t_1:t_2,k} = [s_{t_1,k}, \ldots, s_{t_2,k}]^{\mathrm{T}}$ contains sequential CSQ measurements (*i.e.,* time series) of the same cell k, from time t_1 to t_2. The sampling interval $\triangle t$ is chosen according to some criteria detailed in Appendix A. Measurements are expressed in terms of received signal strength in dB-scale (dBm).

Considering a typical cellular environment, for the idle UE, the CSQ fluctuations $s_{t,k}$ are modeled by a p-th order auto-regressive (AR) model [15] with parameters $\boldsymbol{\theta}_{0,k} = [\mathbf{b}_k, \sigma_k, r_k]$. It is

$$s_{t,k}(\boldsymbol{\theta}_{0,k}) = \mathbf{b}_k^{\mathrm{T}} \times \mathbf{s}_{t-1:t-p,k} + v_{t,k} + r_k \tag{1}$$

where the $p \times 1$ vector $\mathbf{b}_k$ contains the cell-specific AR parameters (here $p = 3$), the residual $v_{t,k}$ models the random log-normal shadow fading fluctuations of link strength, while r_k describes the static CSQ component measured by the UE on cell k and due to cell site-specific path-loss. The residual fluctuations $v_{t,k} \sim \mathcal{N}\left[0, \sigma_k^2\right]$ are represented by a zero-mean Gaussian white stochastic process with standard deviation σ_k.

Considering now a multi-cell environment during a cell reselection procedure, we assume that the CIDs $k \in \mathcal{K}$ belong to the neighbor cell ranking list $\mathcal{K}$. This list contains the cell identifiers suitable to camp on at time t, obtained from the cell reselection criteria. The fluctuations of CSQ $s_{t,k}$, for each cell in $\mathcal{K}$, are described by the AR model (1) with cell-specific[1] parameters $\boldsymbol{\theta}_{0,k} \in \Theta_0$ where $\Theta_0 = \left\{\boldsymbol{\theta}_{0,k} : k \in \mathcal{K}\right\}$.

A change in the environment, *e.g.* an object/person occupying or moving in the area $\mathcal{X}$ in the surroundings of the UE, alters the AR parameters in Θ_0 that are thus replaced with new, but *unknown*, terms $\boldsymbol{\theta}_1 \notin \Theta_0$. The effective geometrical sensing area $\mathcal{X}$ is measured in terms of distance d between the altered target (body/object) and the UE; its influence on detection resolution is discussed in Sect. V based on experimental data. Considering multiple cells $k \in \mathcal{K}$, the data set

$$\mathbf{S}_{t_A:t_B} = \left\{\mathbf{s}_{t_A:t_B,k},\ k \in \mathcal{K}\right\} \tag{2}$$

represents the collection of the anomalous patterns $\mathbf{s}_{t_A:t_B,k}$ induced by a potential change in the interval $[t_A, t_B]$ for all the monitored cells k. Being t_A and t_B the beginning and the end of the change, respectively, each $\mathbf{s}_{t_A:t_B,k}$ consists of $N = (t_B - t_A)/\triangle t$ samples.

B. CELL RESELECTION AND CSQ MEASUREMENT

An in-depth understanding of reselection procedures, as supported by the 3GPP WWAN standards [16]–[19], is instrumental to the design of CSQ analytics for motion detection. This motivates the review herein for self-consistency of the paper. Cell reselection defines a procedure where the UE regularly checks the best cell to camp on according to some RAT-specific ranking criteria. As summarized in the example of Fig. 2 for UTRA WWAN, the general goal of the procedure is to let the UE always camp on a non-barred cell with good enough quality even if it is not the optimal cell at that time. The cell to camp on is top-ranked by the UE based on CSQ $s_{t,k}$ for $k \in \mathcal{K}$ collected on a periodic basis ($\triangle t$), as well as on cell-specific priority ordering criteria that are controlled by the network and regularly published on the Broadcast Control CHannel (BCCH) over the System Information Blocks (SIB). In particular, SIBs contain information about the CID,

[1] We consider here a static cell ranking list (*i.e.,* $\mathcal{K}$ is fixed). The case where new cells add to the list is addressed in the experimental studies of Sect. V.

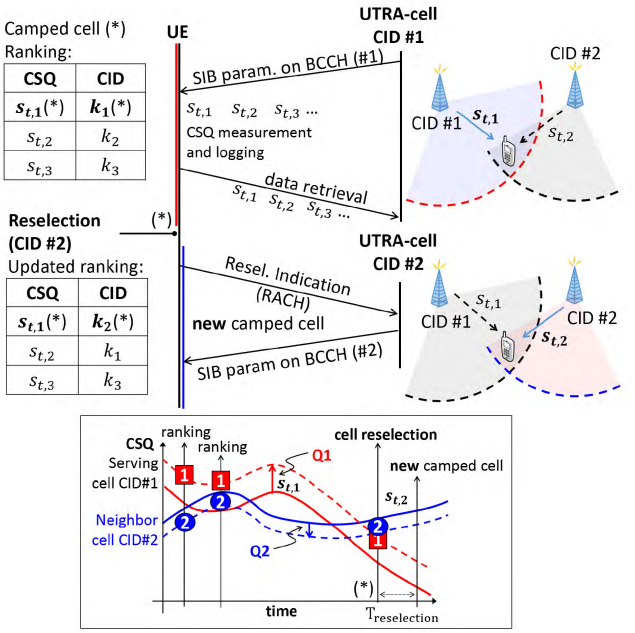

FIGURE 2. Top: simplified message flow diagram for cell reselection according to the UTRA WWAN standard. Bottom: example of cell reselection (*) from serving cell CID#1 to neighbor cell CID#2. CSQ of CID#1 + hysteresis Q1 is compared with CSQ data of CID#2 - Q2 (dashed lines). Reselection decision is delayed by $T_{reselection}$.

barred state, reselection hysteresis/offsets parameters, reselection interval $T_{reselection}$, and CSQ measurement types. Logging of CSQ data may be also retrieved on demand by the network. Once the need for reselection is identified, the UE selects the new highest ranked cell to camp on it through the reselection indication procedure required by the specific WWAN standard.

It is worth noticing that typical WWAN configurations are characterized by a multiplicity of cells for each serving cell-tower or radio network controller (RNC). Cells might correspond to sectors and/or serving frequencies (for GSM/EDGE), one or multiple antennas (for UTRA or E-UTRA), and support multiple RATs. Therefore, the change of cell could imply a change of the radio access protocol. Further details are shown in Appendix A.

Focusing on CSQ measurements, it is important to note that the type and the dynamic range of observable CSQs depend on the specific RAT and network type. For instance, for WCDMA (UTRA), the measure related to the signal strength is known as CPICH RSCP (Common Pilot CHannel Received Signal Code Power) [16] while the measure related to the signal quality is known as CPICH E_c/I_0, namely the received energy per chip E_c of the CPICH divided by the total received power density I_0 in the frequency band [17]. Likewise, for E-UTRA (LTE), the measure related to the signal strength is known as RSRP (Reference Signal Received Power) [18] while an additional signal quality indicator is available as RSRQ (Reference Signal Received Quality) [19]. Arbitrary Strength Unit (ASU) [20] can be typically used as a measure of CSQ values, quantized in 1dB steps for UTRA/E-UTRA and 2 dB steps for GERAN.

TABLE 1. CSQ measurements, CSQ range and ASU range for GERAN, UTRA and E-UTRA WWAN. Notes: (1): ASU values 99 or 255 map to CSQ not known/not detectable; (2): ASU value 0 maps to CSQ < -140 dBm; (3): ASU value -17 maps to CSQ < -156 dBm.

WWAN	CSQ range (dBm)	CSQ	ASU range
GERAN	-113 ÷ -51	$2\,\text{ASU} - 113$	$0 \div 31$ or 99 (1)
UTRA	-120 ÷ -25	$\text{ASU} - 116$	-5 ÷ 91 or 255 (1)
E-UTRA	-156 ÷ -44	$\text{ASU} - 141$	$0 \div 97$ or 255 (1,2)
		$\text{ASU} - 140$	-17 ÷ -1 (3)

Table 1 summarizes the CSQ range and the corresponding ASU to CSQ conversion formulas for current WWAN systems obtained by using the extended cell signal quality AT query command +ECSQ. This command returns the CSQ measurements $s_{t,1}$ of the current camped cell in terms of received signal strength values. It is also possible to use the channel bit error rate (for GERAN), the CPICH E_c/I_0 (for UTRA) and RSRQ (for E-UTRA), even if these latter values are not considered here.

C. AN INTRODUCTORY EXAMPLE: DETECTION OF SPACE UTILIZATION

To better frame the problem, we consider the experimental setting summarized in Fig. 3, that serves as an introductory example as focusing on CSQ inspection on one cell only ($k = 1$), namely the camped cell. A single WWAN-enabled device (a smartphone) is deployed inside a 10 sqm room to detect a human body in the proximity of the UE. In particular, in these tests, the area might be occupied by one human subject that performs non-rigid body motions while sitting at a desk and located at fixed position $\mathbf{x} \in \mathcal{X}$ in the surrounding of the UE. Depending on the body movements, the distance between the UE and the person is $d \leq 1$ m. The CSQs $s_{t,1}$ for time-varying camped cell are collected by the UE over 4 days of continuous data logging in Fig. 3.(a). Signal strength samples are periodically retrieved here on time interval $\triangle t = 5$sec. and expressed in dBm scale, with 2 dB quantization steps. It is apparent that, for the considered device, the serving cell switches among 2 sites here identified by the CID 1280 (for cell $k = 1$) and the CID 3624 (for $k = 2$). In this example, the reselected cells do not correspond to physically separated cell towers, but rather to different serving frequencies of the same tower, identified by the same Location Area Code (LAC), and RNC. Throughout the 4 days trials, the smartphone is fixed in a selected position and thus converted into an always-on passive body motion sensor.

The AR cell signal dynamics $\boldsymbol{\theta}_{0,k} \in \Theta_0$ for the unoccupied environment are here estimated [15] autonomously by the same smartphone during the application initialization. AR parameters are estimated for both CIDs ($k = 1, 2$): for $p = 3$ (AR-3) these are $\mathbf{b}_1 = [0.51, 0.18, 0.3]$, $\boldsymbol{\theta}_{0,1} = [\mathbf{b}_1, \sigma_1 = 1.0\,\text{dB}, r_1 = -64\,\text{dBm}]$, and $\mathbf{b}_2 = [0.65, 0.16, 0.21]$, $\boldsymbol{\theta}_{0,2} = [\mathbf{b}_2, \sigma_2 = 1.1\,\text{dB}, r_2 = -66\,\text{dBm}]$. The two sequences $\mathbf{s}_{t_A:t_B,1}$ highlighted in gray and labelled as (*) and (**), reveal the presence of a moving target in proximity

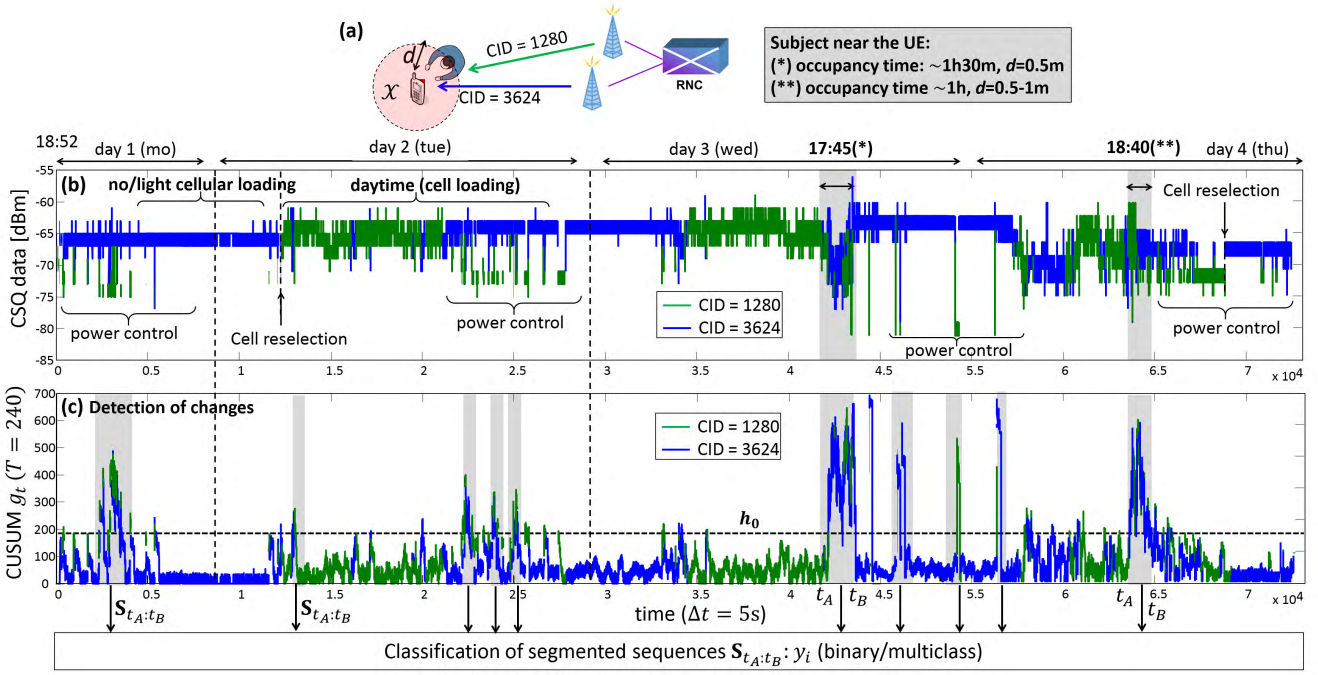

FIGURE 3. From the top: (a) Long occupancy time examples from test measurements: the moving target (human body) is located inside the detection area $\mathcal{X}$, at distance from the UE ranging from 0.5 m up to 1 m. (b): multi-cell CSQ vs. time over 4 days recorded logs. (c): change-point detection cumulative sum g_t with $T = 240$ samples and $\Delta t = 5$ s (for visualization purposes only); threshold is set to $h_0 = 193$.

to the device, with occupancy time and distance d indicated for both cases. Body presence causes small changes of the CSQ dynamics. Other abrupt CSQ variations are clearly visible for the CID 1280 during night-time as caused by network-based power control modifications. These network-induced CSQ changes are not due to body proximity, but rather to network-specific features (*e.g.,* varying cell loading conditions during day-time) that must be detected and filtered out before applying any body/object motion classification algorithm.

The approach followed here for body detection is to first extract (Sect. IV-A) temporal segments $\mathbf{s}_{t_A:t_B,k}$ of *anomalous* CSQ data that might indicate the presence of a moving body in proximity to the UE, as shown in Fig. 3.(b). Then, considering all monitored cells $k \in \mathcal{K}$, every data set $\mathbf{S}_{t_A:t_B}$ in (2) is classified (Sect. IV-B) to discriminate body-induced CSQ changes from others effects such as cell reselection, environmental changes and other network- or cell-induced settings, as shown in Fig. 3.(c).

IV. CSQ PROCESSING AND ANALYTICS FOR DETECTION

The data analytics problem is addressed according to the following two-stage algorithm composed by a sequential change detector followed by a classification stage.

At first, a sequential change detection algorithm is proposed in Sect. IV-A to isolate relevant perturbations in the CSQ dynamics with respect to model (1) and to the cell site-specific parameters $\boldsymbol{\theta}_{0,k} \in \Theta_0$. The algorithm effectively detects small, non-additive, changes that are potentially due to propagation environment perturbation around the UE with the aim to isolate them from *intrinsic* variations clearly attributable to cell-driven re-selection effects, network parameter changes, or other cell-specific modifications. A change point detection method is designed to segment the input CSQ data into the CSQ patterns $\mathbf{S}_{t_A:t_B}$ (2) corresponding to the identified beginning t_A and end t_B of the anomaly.

Next, for the segmented CSQs, a classification stage discriminates true body motions, and more generally body-induced changes in the environment, from other cell-specific effects. Classification of segmented CSQs can be implemented by machine learning methods. More specifically, in Sect. IV-B an ad-hoc Bayesian classifier is proposed. Other tools, namely Support Vector Machines (SVM) and Long-Short Term Memory (LSTM) networks are also evaluated. Bayesian classification leverages on prior modelling and, in some cases, it is less sensitive to the training size. In particular, Bayesian classification adopts a *model space* based on training data or physical body models [21], [22] that are used to characterize the multiplicity of scene alteration configurations in the detection area $\mathcal{X}$. Model averaging is then applied by weighting each model with its probability of being the correct one for the given setting.

The binary classification of environmental changes ($y_i = y_1$) compared to empty space ($y_i = y_0$) is validated in Sect. V. Extension to multiclass classification is demonstrated in Sect. VI for the considered case study.

A. IDENTIFICATION OF CHANGES IN MULTI-CELL SIGNALS

In this section, we investigate the problem of detection and segmentation of changes in multi-cell CSQ signals $s_{t,k}$.

Algorithm 1 Pseudo-Code Fragment of the Sequential CSQ Change Detector

procedure change detection over interval $[t-T, t]$
  for $k \in \mathcal{K}$ **do** ← `all monitored cells`
    for $j = t-T : t$ **do**
      $\ell_{j,k}$ ←`CUSUM (5)`
      $g_t = g_t + \frac{1}{T}\max[0, \ell_{j,k}]$
    end for
  end for
  if (state$(t-1)$ = NO_CHANGE) ← `no changes detected at` $t-1$ **then**
    if ($g_t \geq h_0$) **then**
      $t_A = t$ ←`change start`
      state(t) = CHANGE_DETECTED
    end if
  else
    if ($g_t < h_0$) **then**
      $t_B = t-1$ ←`change end`
      state(t) = NO_ CHANGE
      if ($t_B \geq t_A + T$) **then**
        return $\mathbf{S}_{t_A:t_B}$
      end if
    else
      state(t) = CHANGE_DETECTED
    end if
  end if
end procedure

As previously described, the changes of CSQ dynamics might affect the cell-specific parameters $\boldsymbol{\theta}_{0,k}$ that rule the cell signal dynamics. Given a set of CSQ observations, the proposed sequential change point detection method decides between two composite hypotheses consisting of: *i)* CSQ dynamics, described by parameters $\Theta_0 = \{\boldsymbol{\theta}_{0,k},\ k \in \mathcal{K}\}$, observed by an idle UE from the cells[2] $k \in \mathcal{K}$; and *ii)* post-change dynamics as possibly caused by body/object motions and described by the *unknown* parameter set $\boldsymbol{\theta}_1 \notin \Theta_0$.

Detection problem can be implemented iteratively (on-line) by exploiting the cumulative sum (CUSUM) paradigm. Optimality of CUSUM tests for detection is investigated in [23], [24]. Assuming an inspection interval $[t-T,\ t]$ of duration T, the CUSUM function g_t is defined as

$$g_t = \frac{1}{T}\sum_{k\in\mathcal{K}}\sum_{j=t-T}^{t}\left(\ell_{j,k}\right)^{+} \tag{3}$$

with $\ell_{j,k}$ the log-likelihood ratio terms computed for each cell in the ranking list $\mathcal{K}$ and $(\cdot)^+ = \max[0, \cdot]$. For detection of small changes, the terms $\ell_{j,k}$ simplify as (see Appendix B)

$$\ell_{j,k} \approx \nu \mathbf{u}_1^T \times \mathbf{z}_{j,k}(\boldsymbol{\theta}_{0,k}), \tag{4}$$

[2]It is assumed that knowledge of the cell ranking list is available during the on-line detection process. In fact, this information can be easily extracted from the UE (see Sect. V).

with $\nu > 0$ (here $\nu = 0.2$) and $\mathbf{u}_1$ being a unit vector indicating the predominant *direction* of the change that gives more impact to perturbations of selected model parameters. The $(p+1)\times 1$ score function $\mathbf{z}_{j,k}$ is defined [25] as

$$\mathbf{z}_{j,k}(\boldsymbol{\theta}_{0,k}) = \underbrace{\left[\frac{1}{\sigma_k^2}v_{j,k}\mathbf{s}_{j-1;j-p,k}\right.}_{\text{changes on } \mathbf{b}_k},\ \underbrace{\left.\frac{1}{\sigma_k}\left(\frac{v_{t,k}^2}{\sigma_k^2}-1\right)\right]}_{\text{changes on } \sigma_k,} \tag{5}$$

with the *innovation term* $v_{j,k}$, from (1), is given by $v_{j,k} = \left[1, -\mathbf{b}_k^T\right] \times \mathbf{s}_{j:j-p,k} - r_k$. According to the detection threshold h_0, the beginning t_A and the end t_B of the anomalous sequence are estimated as

$$\begin{aligned} t_A &= \min\{t:\ g_t \geq h_0\} \\ t_B &= \max\{t > t_A + T:\ g_t \geq h_0\}, \end{aligned} \tag{6}$$

respectively. A pseudo-code for the anomaly detection tool is illustrated in the fragment of Algorithm 1.

For the same example considered in Sect. III-C, the CUSUM metric g_t is visualized in Fig. 3.(b) as a function of time t, and for interval (3) equal to $T = 240$ samples. Interval T acts as an adjustable *time control* that can be tuned to trade time resolution for detection area size (d) in order to capture different motion events, according to the specific application. This property is further discussed in Sects. V and VI. The threshold h_0 is chosen here as $h_0 = 193$: optimization of $h_0 = h_0(\varsigma)$ is based on a Constant False Alarm Rate ς (CFAR) approach [26]. Change direction for $p = 3$ is $\mathbf{u}_1 = [\frac{1}{\sqrt{3}}\cos(\frac{\pi}{15}), \frac{1}{\sqrt{3}}\cos(\frac{\pi}{15}), \frac{1}{\sqrt{3}}\cos(\frac{\pi}{15}), \sin(\frac{\pi}{15})]$ as discussed in the Appendix B.

Cell-reselections and other cell-specific network configurations are responsible of *false* alterations of CSQ dynamics with respect to the AR parameters $\boldsymbol{\theta}_{0,k} \in \Theta_0$: these *false* changes, namely not induced by true modifications of the environment around the UE, are addressed during the following classification stage.

B. CLASSIFICATION OF CHANGES

We now discuss how to classify an anomalous CSQ input sequence of N samples $\mathbf{S}_{t_A:t_B}$ (2), from the posterior probability (or belief state) $\Pr\left[y_i|\mathbf{S}_{t_A:t_B}, \mathcal{D}\right]$ that discriminates environment changes hypothesis indicated as y_i, $i > 0$, from the unchanged one (unoccupied space) with class label y_0. The latter hypothesis corresponds to effects that make the CSQ dynamics to deviate from their nominal behavior, resulting in a false change (*i.e.,* false positive).

Classification is here implemented by the UE based on the input CSQ samples and supervised training. Training/example CSQ features $\mathcal{D} = \{\mathcal{D}_i,\ i \geq 0\}$ can be retrieved from a remote data repository, before the actual placement of the UE, at the time of the software installation, and reassigned (by transfer learning) to the application.

Before applying classification, some necessary pre-manipulation of the CSQ data is required to let the detection system be independent from the specific UE or cell deployment as well as to simplify the training stage. Rather than

classifying the segmented time series $\mathbf{S}_{t_A:t_B}$, we choose a more compact data structure by tracking the CSQ deviations

$$\triangle s_{t,k} = s_{t,k} - r_k, \tag{7}$$

between the observed CSQ $s_{t,k} \in \mathbf{S}_{t_A:t_B}$ and the static CSQ component r_k (1) measured during the app initialization (Sect. V-A) for each monitored cell. The counts and the distribution of such deviations are instrumental to classify the potential environment changes. Considering the cell k and the time interval $[t_A, t_B]$, we define the CSQ deviation counts as $\mathbf{f}_{k,Q} = \left[f_{k,1}, \ldots, f_{k,q}, \ldots f_{k,Q}\right]$ where the individual terms $f_{k,q}$ are given by

$$f_{k,q} = \sum_{t\in[t_A,t_B]} \mathbb{I}\left(\triangle s_{t,k} \in \left[\mathrm{v}_{q-1}, \mathrm{v}_q\right]\right), \tag{8}$$

with $f_{k,q} \leq N$ and the bin edges v_q such that $\mathrm{v}_{q-1} < \mathrm{v}_q$. $\mathbb{I}(\cdot)$ is the indicator function. The optimal bin number Q and the edges v_q are obtained from experimental data as shown in Sect. V. Deviation counts provide a useful fixed-length representation that keeps information about CSQ alterations and multiplicity over the considered cell list, but disregards time dependency.

In what follows, we consider 3 different classifiers, these are validated individually for binary and multiclass classification problems in Sects. VI and VI, respectively.

1) BAYESIAN-DCM CLASSIFIER

Bayesian classification depends on prior modelling. Focusing on binary classification, detection of true (y_1) or false (y_0) changes for the input features $\mathbf{f}_{k,Q}$ is conveniently done by branching on the value of the belief $\mathcal{L}_{0,1} = \sum_{k\in\mathcal{K}} \log\left(\frac{\Pr[y_1|\mathbf{f}_{k,Q},\mathcal{D}]}{\Pr[y_0|\mathbf{f}_{k,Q},\mathcal{D}]}\right)$ using a binary decision function $f_{\mathcal{L}_{0,1},\tau_{0,1}} \rightarrow \{0, 1\}$, namely

$$f_{\mathcal{L}_{0,1},\tau_{0,1}} = \mathbb{I}\left(\mathcal{L}_{0,1} > \tau_{0,1}\right) \tag{9}$$

with the optimized threshold $\tau_{0,1}$. Posterior probabilities $\Pr\left[y_i|\mathbf{f}_{k,Q}, \mathcal{D}\right]$ simplify when no prior on class labels is available $\Pr[y_1] = \Pr[y_0]$ as

$$\mathcal{L}_{0,1} = \sum_{k\in\mathcal{K}} \log\left(\frac{\Pr\left[\mathbf{f}_{k,Q}|\, y_1\right]}{\Pr\left[\mathbf{f}_{k,Q}|\, y_0\right]}\right), \tag{10}$$

with $\Pr\left[\mathbf{f}_{k,Q}|\, y_i\right]$ being the conditional density of the deviation counts. A Dirichlet-Compound Multinomial (DCM) model [27] is adopted to represent the distribution $\Pr\left[\mathbf{f}_{k,Q}|\, y_i\right]$ for each class

$$\Pr\left[\mathbf{f}_{k,Q}|\, y_i\right] = \Pr\left[\mathbf{f}_{k,Q}|\boldsymbol{\beta}_{i,k}\right] = \frac{N!}{\prod_{q=1}^{Q} f_{k,q}!} \times \frac{\mathrm{B}\left(\boldsymbol{\beta}_{i,k} + \mathbf{f}_{k,Q}\right)}{\mathrm{B}\left(\boldsymbol{\beta}_{i,k}\right)}, \tag{11}$$

where we recall that N is the number of samples in the considered segment $[t_A, t_B]$ and $\mathrm{B}(\cdot)$ is the the generalized Beta function [28]. The terms $\boldsymbol{\beta}_{i,k} = \left[\beta_{i,k}(1) \ldots, \beta_{i,k}(q), \ldots, \beta_{i,k}(Q)\right]$ act as model hyperparameters: here, these are the expected deviation counts, for cell k, obtained from training data $\mathcal{D}$ and normalized by uniform prior, therefore by setting $\min \beta_{i,k}(q) = 1$. In addition to training, *virtual*, or simulated, counts can be also obtained analytically using the body model detailed in Appendix C. DCM distributions (11) are used to model word burstiness in text recognition [29] while here the same model allows to capture the burstiness of the CSQ deviations induced by true environment changes. Fig. 4.(a) shows 2 example sequences from the data-base $\mathcal{D}_0$ and $\mathcal{D}_1$, corresponding to body occupancy events of 500 s and 400 s, respectively. The (normalized) counts for camped cell $k = 1$, namely $\widehat{\mathbf{f}}_{1,Q}/\sum_{q=1}^{Q} \widehat{f}_{1,q}$, are also reported in Fig. 4.(b) for both sequences. Burstiness of CSQ sequences are clearly visible in Fig. 4.(a): in fact, considering body motion, the subject might be standing or wandering inside the detection area $\mathcal{X}$ for some time, and then changing its posture. Other examples can be found in our open repository [30] featuring 98 different features with $Q = 13$ bins.

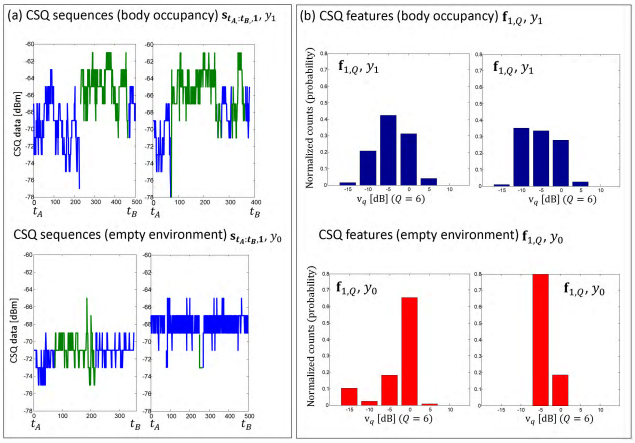

FIGURE 4. (a) Example of 2 CSQ segmented anomalous sequences $\mathbf{s}_{t_A:t_B,1}$ for occupied (y_1 - top) and unoccupied (y_0- bottom) environments extracted from the camped cell with $k = 1$. Green and blue colors correspond to different CIDs; (b) CSQ (normalized) features $\mathbf{f}_{1,Q}/\sum_{q=1}^{Q} f_{1,q}$, for the same camped cell $k = 1$, $Q = 6$ bins and v_q ranging between 15 dB and −10dB (bin size is $\triangle Q = 5$ dB). Training data $\mathcal{D}_i$ are collected from 4 WWAN-enabled devices of different vendors.

In the pseudo-code fragment sketched in the Algorithm 2 for discrimination of occupied and empty environment, namely $y_1 = +1$ and $y_0 = -1$, the decision about body occupancy $\hat{y}_i$ is obtained by evaluating the log-ratio (10) for each cell $k \in \mathcal{K}$ using (11) and then by thresholding. The sensitivity threshold $\tau_{0,1}$ is optimized for the desired performance as shown in Sect. V. Extension of Algorithm 2 to multiclass classification is addressed in Sect. IV-C using a decision-tree policy.

2) SVM CLASSIFIER

The SVM is trained using the same CSQ deviation counts used for Bayesian-DCM. Sequential minimal optimization (SMO) is adopted with regularization parameter $C = 1$ while the other options can be found in [31]. Focusing on binary classification, detection of true and false changes is

conveniently done by assigning the values $y_0 = -1$ and $y_1 = 1$. The classifier

$$\widehat{y}_i = \text{sgn}\left[\omega_0 + \sum_{k\in\mathcal{K}}\sum_m \omega_m \kappa(\mathbf{f}_{k,Q}, \widehat{\mathbf{f}}_{k,Q}^{(m)})\right] \quad (12)$$

uses a Gaussian kernel function $\kappa(\mathbf{f}_{k,Q}, \widehat{\mathbf{f}}_{k,Q}^{(m)})$ with 64 support vectors $\widehat{\mathbf{f}}_{k,Q}^{(m)}$ for which $\omega_i > 0$. sgn$(\cdot)$ is the sign function. Multiclass extension of SVM is investigated in Sect. VI and it is based on an error-correcting output codes (ECOC) model that reduces the problem of multiclass classification to a set of binary classifiers [32]: coding design is one-versus-one.

3) LSTM CLASSIFIER

LSTM is a specific recurrent neural network (RNN) architecture designed to model temporal sequences. Differently from hidden Markov models, it also captures medium/long-term temporal dependencies. LSTM architectures have been thus explored for large scale acoustic modeling in speech recognition, language translation, and handwriting recognition. Focusing on the proposed motion detection problem, LSTM is used to track long and short-term dependencies on the segmented temporal sequences of CSQ. Therefore, unlike Bayesian and SVM tools, LSTM takes CSQ deviation sequences $\triangle s_{t,k}$ in (7) as inputs for all the monitored cells and for segmented intervals $t \in [t_A, t_B]$. Considering an embedded device as target for a practical implementation, the proposed LSTM network is characterized by a limited the number of hidden units and layers. The pre-trained classification network consists of two LSTM layers of 100 and 50 units, respectively, and it is followed by one fully connected (FC) layer, a soft-max and an output classification layer. The first layer weights are pre-trained using a database of CSQ sequences obtained in different settings (see Sect. V) while the second layer weights are trained according to the specific application and the selected number of classes (see Sect. VI). Finally, transfer learning can be also applied on this last layer by freezing the weights of the first LSTM layer. In both cases, learning of weights in each layer is based on the ADAM algorithm [33].

C. DECISION TREE CLASSIFIER FOR BODY PROXIMITY DETECTION

The binary classification of occupancy proposed in the previous section is here reframed into a multi-class detection problem, where true changes from the safe/empty environment scenario ($y_i = y_0$) might be now indicative of environmental changes ($y_i = y_1$) or a more critical body proximity ($y_i = y_2$). We refer to Sect. VI for the description of the specific usage scenario. Multi-class detection is rephrased into a sequence of binary decisions using a decision tree model. This model adopts the Bayesian-DCM tool as a building block to recursively partition the input data space into regions that can be represented by a tree. Similarly to (10), the belief function set $\mathcal{L}_{j,h} = \sum_{k\in\mathcal{K}} \log\left(\frac{\Pr[y_h|\mathbf{f}_{k,Q},\mathcal{D}]}{\Pr[y_j|\mathbf{f}_{k,Q},\mathcal{D}]}\right)$ $\forall j,\ h = 0,\ 1,\ 2$ is selected here as decision tree *attributes*, while we perform branching on the values of these attributes using the binary decision function $f_{\mathcal{L}_{j,h},\tau_{j,h}} \rightarrow \{0, 1\}$ in (9) for the class pair (y_j, y_h) according to the optimized threshold set $\tau_{j,h}$. As the result of such branching operation, the output regions provide a distribution over the class labels $\Pr(y_i|f_{\mathcal{L}_{j,h},\tau_{j,h}})$ $\forall i = 0,\ 1,\ 2$, from which a corresponding decision/alert can be generated similarly as for the binary classification case. Classification trees models are usually easy to implement, in addition, they can efficiently handle heterogeneous data. Decision tree growing and pruning are based here on the C4.5 algorithm (see [34] for a review) while optimization of splitting and thresholds $\tau_{j,h}$ are based on the entropy minimization (or information gain) criterion. Figure 5 shows the actual decision tree generated by C4.5 from training data. It selects $\mathcal{L}_{0,1}$, $\mathcal{L}_{1,2}$ and $\mathcal{L}_{0,2}$ as attributes and the corresponding optimized thresholds $\tau_{0,1}$,$\tau_{1,2}$ and $\tau_{0,2}$ are highlighted.

Algorithm 2 Pseudo-Code Fragment of the Anomaly Classifier

procedure classification of sequence $[\mathbf{S}_{t_A:t_B}, \{r_k, k \in \mathcal{K}\}; \boldsymbol{\beta}_{i,k}]$
  for $k \in \mathcal{K}$ **do**← all cells in the ranking list
    for $q = 1 : Q$ **do**
      $\triangle s_{t,k} = s_{t,k} - r_k$
      $f_{k,q} = \sum_{t\in[t_A,t_B]} \mathbb{I}\left(\triangle s_{t,k} = \text{v}_q\right) \leftarrow \mathbf{f}_{k,Q}$
    end for
    $\mathcal{L}_{0,1} = \mathcal{L}_{0,1} + \log\left(\frac{\text{B}(\boldsymbol{\beta}_{1,k}+\mathbf{f}_{k,Q})\text{B}(\boldsymbol{\beta}_{0,k})}{\text{B}(\boldsymbol{\beta}_{1,k})\text{B}(\boldsymbol{\beta}_{0,k}+\mathbf{f}_{k,Q})}\right)$ ←in (10) and (11)
  end for
  $\hat{y}_i = f_{\mathcal{L}_{0,1},\tau_{0,1}} \leftarrow$ false $\hat{y}_i = y_0$ if $f_{\mathcal{L}_{0,1},\tau_{0,1}} = 0$ otherwise true $\hat{y}_i = y_1$
end procedure

V. EXPERIMENTAL VALIDATION

In order to verify the performances of the proposed approach, we conducted a one-month case study in an indoor site, using 4 different smartphones with SIM cards from two different mobile operators. The study is meant to compare the CSQ data processing tools for motion detection considering various environment alterations ranging from body motions to long-term changes of the environment surrounding the smartphone. We also address the sensitivity area size d [21], [22] and CUSUM interval T, that rules the time resolution for anomaly detection (Sect. IV-A). For all cases, we used COTS devices with WWAN modem chips from different manufacturers. Considering each UE, the system is able to track CSQ data measured from 3 neighboring cells, being $k = 1$ the camped cell, while $k = 2,\ 3$ are the 2nd and 3rd strongest cells in the ranking list, respectively.

As highlighted in Sect. IV-A, the CUSUM interval T serves as an adjustable control parameter that can be tuned to adapt the anomaly detection capability and resolution. Fig. 6 shows

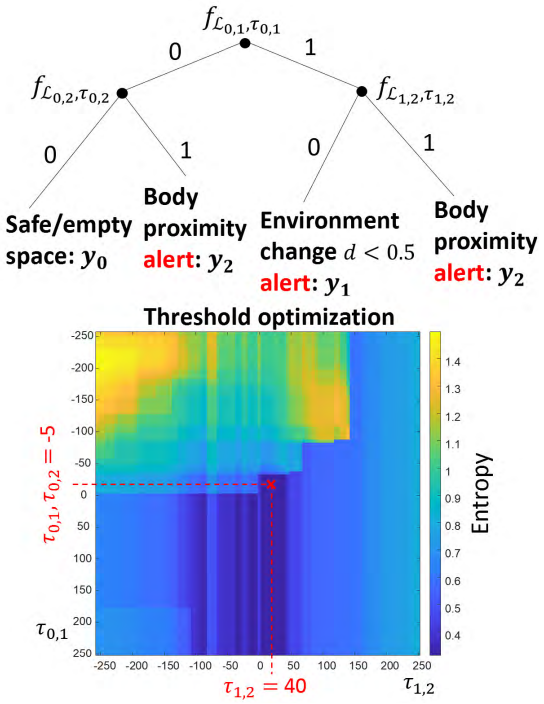

FIGURE 5. Detection and classification of *i*) body proximity (y_2), *i.e.,* for detection of possible tampering attempts; *ii*) environment alterations (y_1) in the surrounding of the smartphone and *iii*) empty (unoccupied) environment (y_0). Decision tree, thresholds $\tau_{0,1}$, $\tau_{0,2}$ evaluation and threshold $\tau_{1,2}$ optimization using training data are shown.

two selected CSQ data-sets. The first one (case #1 on the left) considers the detection of body motions, the second one (case #2 on the right) consider the detection of long-term space utilization. The first case addresses the detection capability of individual body motions of short-time, between $2 \div 6$ min. This is relevant in applications that require an accurate estimation of the entrance time t_A of the subject. Space utilization addressed in the second case refers to the detection of the occupation time $T_{A-B} = t_B - t_A$ to determine how often a space is occupied. Detection of such events is typically important in a variety of smart living applications, including access, intrusion [35] and behavioral routine monitoring, energy-efficient heating ventilation, and lighting [36], [37].

Considering the above scenarios, in Fig. 6 the corresponding CUSUM g_t outputs (3) for $T = 60$ and $T = 190$ are compared. Detected anomalies, for which $g_k \geq h_0$, are highlighted in gray. For target moving close to the UE ($d \leq 0.5$ m), body-induced effects on CSQ data are, in many cases, evident (case #1) while detection of short occupation times, above 2 min, is possible provided that the detectable interval, i.e., $T = 60$, is kept small enough to minimize false negatives. For more distant subjects ($d = 0.5 \div 1$ m) body effects are less evident, but still observable when the subject moves around for longer time ($>$ 10 min, see case #2 at bottom). A small CUSUM interval T provides an accurate estimation of the entrance time t_A of the subject into the detection area, in exchange for a less precise evaluation of the occupation time, namely $T_{A-B} = t_B - t_A$. A larger interval, $T = 190$ in the example, should be therefore preferred for more accurate estimation of T_{A-B} intervals, when needed for the specific application. This tradeoff is further explored in the following sections.

A. INITIALIZATION: LEARNING AND CLASSIFICATION

The proposed proof-of-concept approach for body motion detection combines an anomaly identification method with a classification stage to discriminate body movements from other network-related effects. For anomaly detection, learning of device-specific propagation parameters Θ_0 and CFAR value ς is required, from which the threshold level $h_0 = h_0(\varsigma)$ can be obtained. On the contrary, training data for classification is based on labeled example features $\mathcal{D}$ of typical CSQ deviations (measured or simulated), indicating body motions in the surroundings of a UE. These features $\mathcal{D}$ are pre-configured, independent of the device and can be retrieved from the cloud repository [30] so to implement transfer learning approaches.

1) ON-LINE LEARNING OF CHANGE DETECTOR PARAMETERS

AR parameters Θ_0 describe the dynamics of the cell signals for unoccupied detection area and depend on the UE location. For the considered case study, the initial calibration of Θ_0 is carried for approx. 1 h (*i.e.,* during night-time). Notice that a new calibration should be carried out when moving the UE to a different location (*e.g.,* a new room or building) or when the cell ranking list contains new sites, unless these sites are excluded from the list. According to Sect. IV-A, the CFAR ς determines the threshold h_0 above which an anomaly can be considered relevant for body detection. For an assigned CFAR value ς, threshold $h_0(\varsigma)$ is computed locally by the UE as $h_0(\varsigma) = \{h_0 : \Pr[g_t \geq h_0] = \varsigma\}$ and based on the CUSUM g_t (3) obtained from the same training CSQ data used for parameter Θ_0 estimation. As analyzed in the followings, CFAR values are optimized for detection of long/short events.

2) MODEL SPACE AND FEATURES FOR CLASSIFICATION

Defined in Sect. IV-B, the Bayesian-DCM classifier uses the hyperparameters $\boldsymbol{\beta}_{i,k}$ that are the CSQ deviation counts obtained from the training data $\mathcal{D}$. The database $\mathcal{D}$ is available online [30] and consists of $M = 98$ training sequences with $Q = 13$ bins ($-15 \div 9$ dB) and bin size $\triangle Q = 2$ dB. The same features are used to train the SVM classifier. The hyperparameters computed from training can be also combined with simulations obtained by electromagnetic (EM) body modelling (Appendix C). Training of the LSTM network is based on the same CSQ deviation sequences $\triangle s_{t,k}$ of length T_{A-B} used to compute the above mentioned counts.

B. MONITORING OF SPACE UTILIZATION

In the field of assisted living (and working), it is often important to quantify the utilization of space and occupation times,

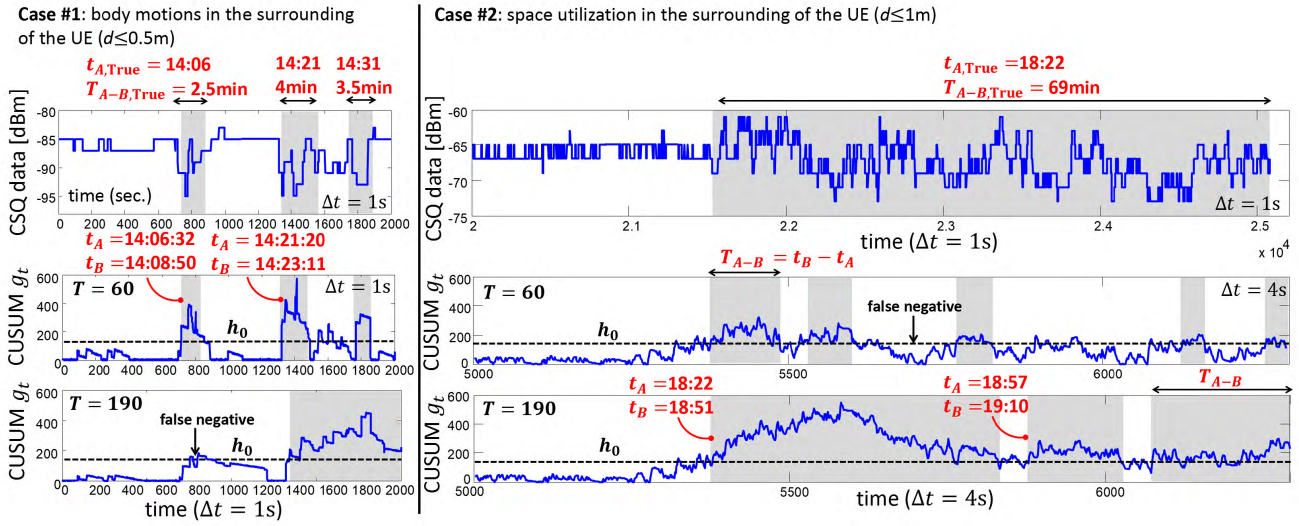

FIGURE 6. Effect of the CUSUM interval T on the anomaly detector. From top to bottom: measured CSQ data from device A (cell reselections are omitted for clarity), corresponding CUSUM g_t functions for the same CSQ data but with different T setting equal to $T = 60$ and $T = 190$. Different occupancy events are considered: case #1 (left) highlights 3 short occupancy events of $2 \div 4$ min, case #2 (right) focuses on a long occupation time (1 hour). Estimated subject entrance time t_A and occupation ($T_{A-B} = t_B - t_A$) for each detected anomaly are superimposed. The corresponding true occupancy time $t_{A,\text{True}}$ and duration $T_{A-B,\text{True}}$ are reported on top.

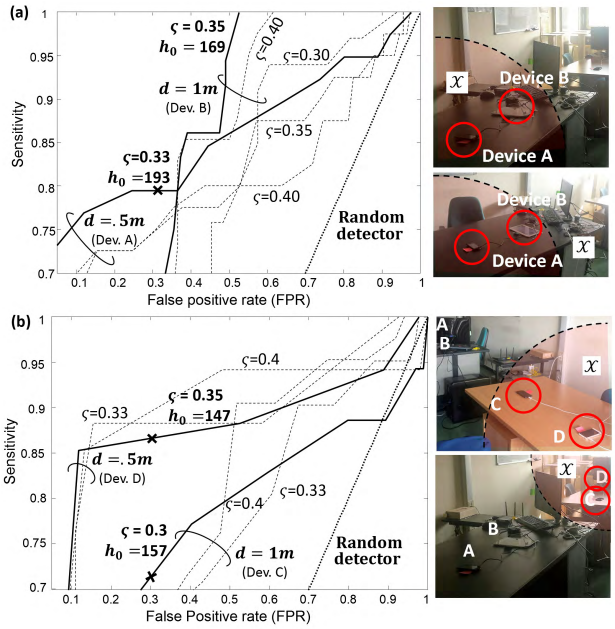

FIGURE 7. ROC curves for the Bayesian-DCM classifier using (a) devices A, B and (b) devices C, D for varying CFAR values ς: the optimized value for FPR$\leq$ 0.3 is shown in bold. These curves are computed based on 15 day tests for devices A, B and 12 days for devices C, D. The layout for all tests is depicted on the right. Performances of the random detector are also shown for comparison.

especially if they are unusually long [36], [37]. For example, in social interaction sensing applications [38], information about long/frequent occupations can be used for optimization of physical spaces or even to profile the interest of an object (*i.e.,* in smart retail applications). A proof-of-concept is developed in this section to address the detection capability using cellular signals under such requirements. In particular, 32 different occupancy scenarios were tested over a period of 30 days with 1-2 occupancy events per day, characterized by a minimum time of 30 min and maximum of 2 h. Ground truth videos as well as corresponding timestamps are recorded for each event to allow for correct data labeling. Considering such events, CSQ samples are here retrieved with sampling time $\Delta t = 4$ sec. and detectable interval equal to $T = 192$ (corresponding to $T \times \Delta t = 13$ min). The Receiver Operating Characteristic (ROC) curves [26] are depicted in Fig. 7 for the Bayesian-DCM classifier. They compare sensitivity vs. False Positive Rate (FPR) for all tests. These are analyzed for varying CFAR values ς. Performance of the random binary detector (*i.e.,* trivial detector) is also shown. In Fig. 7.(a), the devices A, B monitor the same area (a) depicted on the right, where the target moves at a maximum distance d equal to 0.5 m, 1 m and 2 m from each UE, respectively. In Fig. 7.(b), the devices C, D sense a different area where the target moves at a distance d up to 1 m and 0.5 m, respectively. Optimal CFAR values for each case are highlighted in bold and are chosen here to maximize sensitivity subject to a maximum FPR equal to 0.3 (see the corresponding markers). Optimal CFAR values fall within the same interval $0.3 \div 0.35$ depending on the device position, but they map to different threshold values. According to the above choice, anomaly detector threshold is set to $h_0 = 2$.

Figure 8 compares accuracy, precision and recall (sensitivity) rate for varying detection interval values T by considering, for all devices, the same CFAR configuration ($\varsigma = 0.3$). Results for Bayesian-DCM classifier (solid lines) and SVM tool (dashed lines) are compared. Considering both methods, precision (counting false positives) remains high ($\geq$ 0.85)

TABLE 2. Motion detection performances vs. body distance d for device A and B.

Body distance [m]	≤ 0.5	$0.5 \div 1$	$1 \div 2$
Accuracy	0.91	0.66	0.47
Negative Predictive Value (NPV)	0.96	0.85	0.74

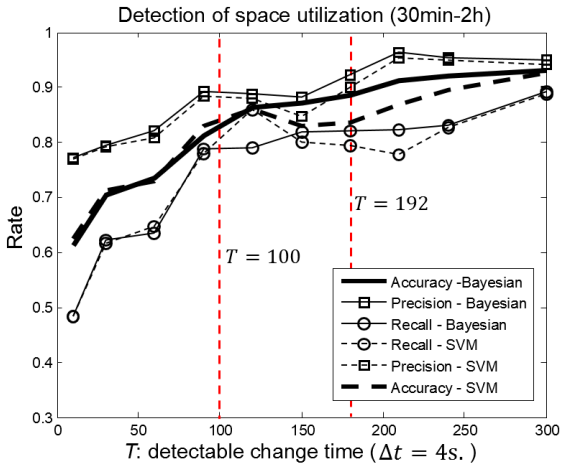

FIGURE 8. Bayesian-DCM classifier (solid lines) vs. SVM tool (dashed lines) results in terms of accuracy, precision and recall (sensitivity) rate for varying detectable change time T expressed in number of samples (notice that $\Delta t = 4$ s). Devices A, B, and C, D are considered with configuration parameters $\varsigma = 0.3$ (corresponding anomaly thresholds h_0 are in Fig. 7) and $h_{0,1} = 2$.

for the considered intervals T. However, sensitivity drops for $T < 100$ (*i.e.,* 10 min) as caused by a large number of false negatives.

Tab. 2 highlights the motion detection capability for varying distance $d = 0.5 \div 2$ m of the body from the smartphone. For $d \geq 1$ m, accuracy, counting both true-positives and negatives out of total calls, drops below 50% thus posing an upper-limit of $d = 2$ m on the detection range. Body movements in close proximity to the UE ($d \leq 0.5$ m) can be detected with average accuracy of 0.91, while accuracy falls to 0.66 for distances $0.5 \leq d \leq 1$ m. Notice that the detector still correctly identifies false anomalies as evident from the corresponding Negative Predictive Value (NPV) [26], counting true-negatives out of total negative calls: this property is promising for applications related to proximity-based localization.

Finally, for current 3G/4G devices, it is already possible to exploit lower CSQ sampling intervals Δt in the range of 200 ms and this limit will be exceeded in future low-latency 5G networks. In this case, it will be theoretically possible to detect short occupancy events below the 30 sec. limit. In the following section, we explore this scenario by developing an ad-hoc Android app and the related computing platform.

VI. A CASE STUDY: IS SOMEONE APPROACHING MY SMARTPHONE?

The possibility of turning a smartphone into a virtual motion sensing device through the sole use of the cellular modem has several potential applications that can benefit from the proposed configuration and the ubiquitous diffusion of WWAN devices. For example, the availability of such paradigm gives off-the-shelf smartphones the ability to sense its surrounding space and, in turn, enable proximity based services.

Motivated by the above results, we now focus on an application-specific case study. The UE signals are here monitored to transform the smart-device into a flexible sensor for detecting and discriminating body motions in close proximity to the device, from environmental changes happening at larger distance form the UE. The case study is relevant in the field of intrusions [38] and detection of tampering attempts. The CSQ processing tools analyzed in the previous sections serve here as basic building blocks to provide a finer grained classification of the environmental alterations surrounding the smartphone. In fact, the purpose is now to estimate the presence of a body in close proximity $d < 0.25$ m as possibly indicating a malicious tampering attempt on the device and then discriminate this situation from other body-induced changes of the surrounding environment ($d > 0.25$ m). In some cases, this might be indicative of a side channel attack [39]. To address such problem, 177 "tampering attempts" scenarios were simulated and tested with real CSQ data over a period of 3 days using the same devices A, B shown in Sect. V. Out of these tests, 59 tests represent side channel attack attempts where a person is moving around the UE and traversing the detection area from different directions while 59 sets refer to an empty/safe area. Finally, the last 59 tests represent a potential attacker in close proximity $d < 0.25$ m to the device so to raise critical alerts.

Based on such measurements, we developed a demonstrator of the system[3] based on an Android application. In particular, the system triggers an alert (y_1) when a person is approaching the target device, *i.e.,* the UE itself, or a device located nearby. On the contrary, a more critical body proximity alert (y_2) is raised in correspondence with the identification of a prolonged alteration of the scene surrounding the target device ($d < 0.25$ m), where the attacker might take physical control of the device [40] (*e.g.,* by installing malicious applications, compromising the bootloader, or extracting sensitive information about recent user inputs). This situation might also cause unusual cell network activity (*i.e.,* frequent reselections). The scenarios, including the empty/unoccupied space (y_0) are represented visually in Fig. 9 using selected snapshots from the demonstrator. Video records of the demonstrator are further described in the following sections.

A. DEMONSTRATOR: REAL-TIME PROCESSING OF CELL DATA

As depicted in Fig. 9, the body motion alerts are made accessible remotely by an end-user application running on a portable device and interfacing with a cloud server.

[3] Video records available at https://youtu.be/8fk8zxW0g8c, 27 June, 2018.

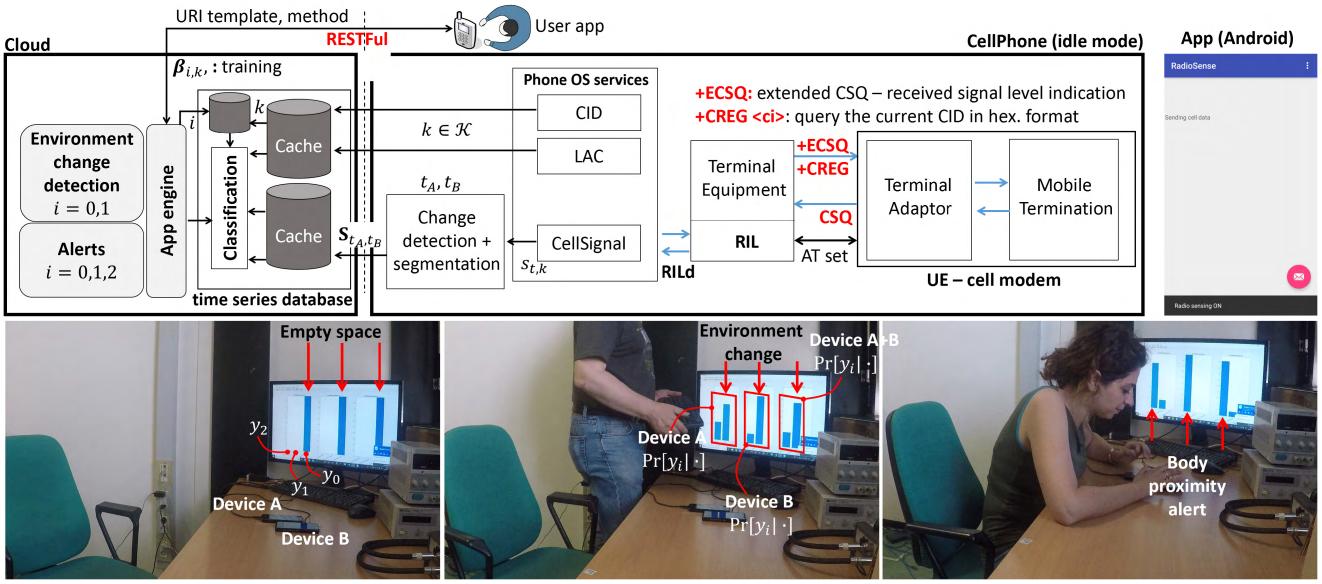

FIGURE 9. Top: computing architecture and cell data retrieval model. Bottom: real-time demonstrator snapshots for detection of unoccupied room (y_0), environment change (y_1) and body proximity (y_2) using two smartphones (Device A and B). For each device, the classifier output is represented visually by posterior probabilities $\Pr[y_i|\mathcal{D}]$.

The cloud platform exposes a set of *REST APIs* (Representational State Transfer) that are used by 2 smartphones (devices A, B) to send the monitoring data encoded in a *JSON* (JavaScript Object Notation) format. Real-time measurements of CSQ are done by each smartphone individually: they are based on the Radio Interface Layer (RIL) that provides an interface between the upper-layer telephony services and the radio hardware layer. Focusing on a typical Android platform implementation, android.telephony provides APIs[4] and abstract base classes for monitoring the basic cellphone information, including CSQ, network type and CID information by communicating with the RIL daemon (RILd). The RIL adopts both standard and proprietary AT commands to interact with the modem functions, via a virtual serial line interface (UART) port. As depicted in Fig. 9 (on top), the 3GPP command AT+ECSQ [20] can be used by the RIL driver to retrieve the received signal strength indication (see also Tab. 1) measured from the current camped cell by controlling the Mobile Termination (MT) vendor-specific functions from the Terminal Adapter (TA) interface.

The data set obtained from the RIL and used for anomaly detection and classification contains the list of surrounding cells, and for each cell: the CID information, the LAC code, the CSQ $s_{t,k}$ measured in dBm and the selected RAT. Currently, the demonstrator supports GSM, UTRA and LTE cells (when available) requiring a level of Android API greater or equal to 18. Considering UTRA and LTE cells, CSQ measurements are reported to the RIL with $\Delta t = 200$ ms measurement period (see Appendix A). This small reporting period is used to capture fast motions, still with good resolution. Processing of CSQ is based on adjustable control parameters (interval T, CFAR ς), that should be tuned to capture application-specific events. For the specific case study, the CFAR for anomaly detection is increased to $\varsigma = 0.4$, while according to the analysis in Sect. V, setting $T = 100$ provides a good tradeoff between accuracy and time resolution.

Selected snapshots of the video records are depicted in Fig. 9. The system is configured to discriminate between unoccupied room (y_0), environment change (y_1) and body proximity (y_2) using 2 devices. Detected anomalies are fed back to the cloud platform through the REST API 'POST /api/postRadioData' for classification. The video shows two simulations of body proximity and environmental changes that involve two different people. In particular, environmental changes are due to a person moving around the smartphones and/or moving objects (*i.e.,* a keyboard or a computer). Body proximity alerts are generated in correspondence of a person sitting at a desk and attempting to extract information from device B. From the video records, the time delay (latency) between a true body movement and its corresponding detection time ranges between 15 sec. and 20 sec.: notice that, beside anomaly detection and classification time, JSON object serialization/deserialization processes add a small but not negligible delay.

B. VALIDATION: ENSEMBLE MODEL AND COMPARATIVE ANALYSIS

We use an ensemble method to combine different models with the goal of improving the robustness over a single estimator. The proposed ensemble model exploits the output of 3 classification algorithms, namely Bayesian-DCM, SVM and

[4] Similar APIs are provided by other platforms *i.e.,* iOS, Windows Mobile, although not considered here.

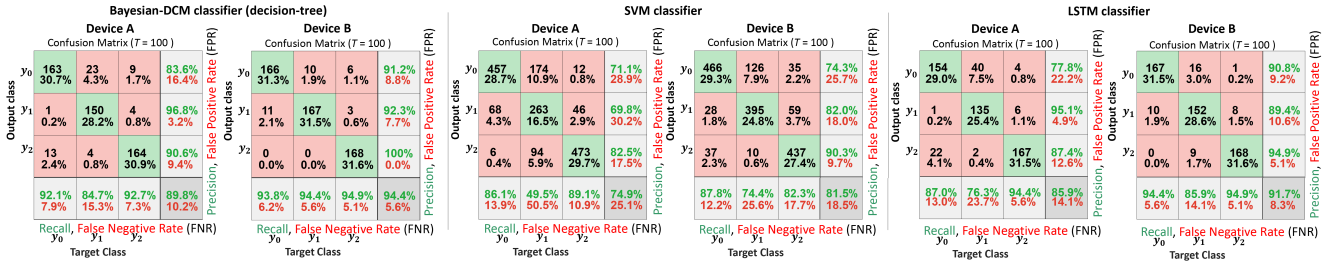

FIGURE 10. Confusion matrices for decision-tree classifier (based on Bayesian-DCM modelling) and comparison with SVM and Long Short-Term Memory (LSTM) classifiers. Matrices are computed over 477 tests and using a time interval of $T = 100$ samples (corresponding to 20 sec., being $\Delta t = 0.2$s). Average accuracy, precision and recall for all classes y_0, y_1, y_2 are also highlighted.

LSTM to generate alerts (Sect. IV-C). The model outputs a measure of the posterior probabilities $\Pr[y_i|\mathcal{D}]$ for each class, such that $\Pr[y_i|\mathcal{D}] = \frac{1}{3}\left(\hat{y}_{i,\text{SVM}} + \hat{y}_{i,\text{Bayesian-DCM}} + \hat{y}_{i,\text{LSTM}}\right)$ where $\hat{y}_{i,\text{SVM}}$, $\hat{y}_{i,\text{Bayesian-DCM}}$ and $\hat{y}_{i,\text{LSTM}}$ are the outputs of the individual classifiers, respectively. A decision about a specific alert can be made by maximizing over the posterior $\hat{y}_i = \text{argmax}_i \Pr[y_i|\mathcal{D}]$. Other models, *i.e.,* sequential- or boosting-based, can be also applied as well [41]. To highlight the comparative analysis among different devices, posteriors are obtained using CSQ data from device A and B, first separately and then jointly.

The three classifiers are now analyzed separately using the CSQ data collected from 3 different people. In Fig. 10, we analyzed and compared the performance of the three selected classifiers in terms of precision, recall and total accuracy. In particular, the Bayesian-DCM classifier is now based on the decision tree structure optimized in Sect. IV-C. Fig. 10 compares the confusion matrices obtained for device A and B separately assuming $T = 100$ samples as minimum detectable change time (corresponding to 20 s for $\triangle t = 200$ ms). The decision tree classifier, based on Bayesian-DCM modelling, is characterized by an average accuracy of 90% that is comparable with the LSTM classifier. Observed accuracy of the SVM detector is slightly lower (80%). Body proximity involve a prolonged alteration of the scene in close proximity to the device with $d \leq 0.25$ m; classifiers are thus characterized by better precision and recall performance. As confirmed by the tests of Sect. V, Bayesian-DCM can correctly discriminate between body movements (classes y_1,y_2) and unoccupied environment (y_0) with accuracy larger than 83% considering both devices. Separation of specific movements (y_1) from proximity (y_2) of the subject can benefit from the use of an ensemble classifier that combines individual weak learners. Notice that, as expected, the classifiers running on device B, target of the tampering attempts during the tests, gives better performances than device A (that is not directly tampered).

VII. CONCLUDING REMARKS

This research aims to introduce the use of cellular radios for human sensing, to detect body occupancy and movements in a confined space as well as their evolution in space and time. Techniques for CSQ analysis are thus proposed to map distinctive anomalous CSQ footprints onto potential movements of people in the surrounding of the smartphone. A proof-of-concept real-time demonstrator has been developed to check the system feasibility. Experiments have been carried out over a period of one month of continuous usage, considering from 2 to 4 cellular devices and different body occupancy configurations over long and short occupation times. The system is able to detect specific body motions, as indicators of possible tampering attempts on device. In particular, the paper addressed the discrimination of body proximity from environmental changes made in the surroundings of a smartphone ($d \leq 0.5$m).

Based on the developed demonstrator, CSQ analysis can be implemented inside the UE (i.e. for decision tree and binary classification) while more complex computations can be also carried out on a back-end (or cloud) component and then retrieved by the end user on demand. All application based on CSQ inspection can run in the background to enable always-on sensing without any explicit user intervention (as far as the smartphone is turned on, mainly in idle mode) and with less significant stress on the battery life compared to conventional solutions that often require supplementary sensors or long sleep periods [37].

With the improved processing power of current evolved cellular devices, as well as denser networks and multiple RATs, new, even unexpected, applications could also emerge by exploiting this novel opportunity. For example, the adoption of large-scale cell signal fluctuation analysis from multiple smartphones might be explored for the localization of movements (e.g., moving people) and crowd sensing/counting applications, combining the multitude of radio signals exchanged by the cellular radio devices. Other classifiers might be also designed on top of the proposed anomaly detection tool to discriminate more specific body motions, such as friction-less body gestures, user habits, frequent activities or social interactions. Devices supporting dual-sim in full active mode can be also employed to increase the number of monitored links and thus the precision. Furthermore, it is useful to mention that the CSQs are also signaled to the network for mobility management by a (large) population of UEs. Therefore, all functionalities highlighted in this paper

for UE-centric system can be carried out at network level with some straightforward adaptations.

APPENDIX A
CELL RESELECTION

For normal service in *idle mode*, the UE regularly and autonomously monitors the BCCH to receive system information from the public land mobile network (PLMN): this include any updated reselection parameters that are published on SIB 1, 2, 3, 4, 7, and 11. The number of cell reselections over time can be controlled by the network operator through time-to-trigger and a hysteresis parameters. These parameters are typically unique for the serving cell. The UE compares the CSQ measurements performed on the applicable frequencies according to a ranking criterion in order to select the best cell. Finally, it autonomously reselects to the chosen cell according to reselection criteria and the network parameters after having verified the cell accessibility. Notice that, when engaged in communication sessions (*i.e.,* in the *active mode* state), the UE is under the full control of the network, and the handover procedures are applied for reselection. In this case, decisions are thus taken only by the network according to the CSQ measurements collected by the UE.

Considering the relevant case where the UE is capable of communicating with multiple RATs and in the area where the UE is camped there are multiple networks, cell reselection is based in general on intra-frequency, inter-frequency and inter-RAT selection criteria. The UTRA and E-UTRA cases are summarized in the following paragraphs (see [14] for GERAN networks).

UTRA (UMTS) case. The received signal strength level is estimated according to the RSCP value that denotes the power measured by a receiver on a particular physical communication channel (or spreading code). At least 2 measurements must be used for the received signal strength estimate. The UE shall scan all RF channels in the UTRA bands according to its capabilities to find available PLMNs. Focusing on typical FDD cell, the UE selects the PLMN that has measured primary CPICH RSCP value greater than or equal to -95 dBm. Once a PLMN has been selected, the UE must choose an acceptable or suitable cell to camp on. The method adopted for cell selection is based on the S-criterion that exploits the measured cell quality $Q_{qualmeas}$ and the measured cell receiver level $Q_{rxlevmeas}$ values [17]. These measurements are based on the CPICH E_c/I_0 and CPICH RSCP, respectively. When camped, the UE decodes the applicable SIB values and performs all relevant signal measurements in order to execute the cell reselection procedure. The ranking method adopted for cell reselection is based on the R-criterion [17]. It uses the results obtained from the S-criterion to select a new cell that has a ranking greater than the servicing cell during the assigned time interval $T_{reselection}$. The UE is capable of monitoring [16] up to 32 intra-frequency cells and 32 inter-frequency cells given in the cell information lists found in the SIB. Up to 8 neighboring cell measurements are reported to the higher layers with a 200 ms measurement period.

E-UTRA (LTE) case. CSQ measurements are based on the computation of the RSRP and RSRQ values of the serving and neighboring cells that are periodically obtained by UEs via detection of reference signals [14]. As already shown for the UTRA case, the UE scans all RF channels of the E-UTRA bands to select a high quality PLMN that has the measured RSRP value greater or equal to -110 dBm. When camped on a cell and in idle state, the UE tries to detect, synchronize and collect at least 2 RSRP and 2 RSRQ samples to compute the power measurements from intra- and inter-frequency neighboring cells. The cell reselection procedure is similar to the one already described for the UTRA case: however, $Q_{qualmeas}$ and $Q_{rxlevmeas}$ are now based on the RSRP and RSRQ values, respectively [19]. The cell reselection timer $T_{reselectionRAT}$ used by the S-criterion is chosen according to the used RAT (*e.g.,* $T_{reselectionEUTRA}$ for the E-UTRA case). This value, and all other parameters used by the UE, are specified in the system information set that is broadcast by the serving cell. Finally, the UE performs ranking of the cells according to the R-criterion [19] that exploits the RSRP values only. The best ranked cell is then used for reselection.

APPENDIX B
CHANGE-POINT DETECTION

The sufficient statistics for the specific detection problem is the generalized likelihood ratio defined as

$$\ell_{t,k}(\boldsymbol{\theta}_{0,k}) = \sup_{\boldsymbol{\theta}_1 \in \Theta_1} \left(\ln \left[\frac{\Pr_{\boldsymbol{\theta}_1}\left(s_{t,k}|\mathbf{s}_{t-1:t-q-1,k}\right)}{\Pr_{\boldsymbol{\theta}_{0,k}\in\Theta_0}\left(s_{t,k}|\mathbf{s}_{t-1:t-q-1,k}\right)} \right] \right) \tag{13}$$

being the supremum computed over the (unknown) parameter set $\boldsymbol{\theta}_1 \in \Theta_1$ and function of the change time. $\ln(\cdot)$ is the natural logarithm function. The movements of the body in the surroundings of the UE cause small changes of the CSQ dynamics $\boldsymbol{\theta}_{0,k}$ observed for the empty environment, and modeled as

$$\boldsymbol{\theta}_1 \approx \boldsymbol{\theta}_{0,k} + \nu \mathbf{u}_1 \tag{14}$$

with $\nu > 0$ and $\mathbf{u}_1$ being a unit vector indicating any prior information (if available) of the predominant direction of the change. Using this local hypothesis assumption [25], the likelihood ratio simplifies as

$$\begin{aligned} \ell_{t,k} &\approx \nu \mathbf{u}_1^T \times \frac{\partial}{\partial \boldsymbol{\theta}_1} \ln \left[\frac{\Pr_{\boldsymbol{\theta}_1}\left(s_{t,k}|\mathbf{s}_{t-1:t-q-1,k}\right)}{\Pr_{\boldsymbol{\theta}_{0,k}\in\Theta_0}\left(s_{t,k}|\mathbf{s}_{t-1:t-q-1,k}\right)} \right] \Bigg|_{\boldsymbol{\theta}_1=\boldsymbol{\theta}_{0,k}} \\ &= \nu \mathbf{u}_1^T \times \frac{\partial \ln \Pr_{\boldsymbol{\theta}_1}\left(s_{t,k}|\mathbf{s}_{t-1:t-q-1,k}\right)}{\partial \boldsymbol{\theta}_1} \Bigg|_{\boldsymbol{\theta}_1=\boldsymbol{\theta}_{0,k}} \\ &= \nu \mathbf{u}_1^T \times \mathbf{z}_{t,k}(\boldsymbol{\theta}_{0,k}) \end{aligned} \tag{15}$$

where the score function $\mathbf{z}_{t,k}$ is defined in Sect. IV Eq. (5). In absence of any prior information about the vector $\mathbf{u}_1$, as assumed in this paper, it can be selected to give more impact on changes whose direction is orthogonal *i.e.,* $\mathbf{u}_1^T \mathbf{u}_0 = 0$, to

the change direction $\mathbf{u}_0$ observed in the empty environment (that would result in false positives):

$$\mathbf{u}_0 = \text{argmin}_{\mathbf{u}, t\in[t-T,\ t]}\,(g_t) \quad \text{s.t. } g_t \leq h_0 \tag{16}$$

APPENDIX C
EM MODELLING OF DCM PARAMETERS

We consider an analytical model to be used as prior information for body presence recognition and for evaluation of the DCM hyperparameters $\boldsymbol{\beta}_{i,k}$. Considering body motions as target for classification, we first evaluate numerically the probabilities $\Pr\left(\triangle s_{t,k} \in \left[\mathrm{v}_{q-1}, \mathrm{v}_q\right] | \mathbf{x}, y_i\right)$ of observing the CSQ deviations $\triangle s_{t,k}$ for random body postures in $\mathbf{x} \in \mathcal{X}$. An EM body model is considered [21], [22]: the human body is approximated as a 3D homogeneous absorbing cylinder placed on the floor, with height $h = 1.8$ m and having an elliptical base with semi-axes $\mathrm{a}_{yu} = 0.55$ m and $\mathrm{a}_{yv} = 0.25$ m. The 3D cylinder could rotate along the vertical axis by the angle ϑ to mimic a person standing in a specific position $\mathbf{x} \in \mathcal{X}$ but changing its orientation. To simplify the complete 3D model, the cylinder is sketched as an EM equivalent 2D knife-edge absorbing surface that can be easily modeled according to the scalar Fresnel-Kirchoff diffraction theory. For a downlink path of length $D_k \gg d$ connecting the UE to the cell tower antenna k, the CSQ deviations $\triangle s_{t,k}$ can be simulated numerically, since they depend, in first approximation, on the geometrical size of the person, its position $\mathbf{x} \in \mathcal{X}$ and the posture/orientation ϑ, with respect to the UE and the downlink path [22]. Posture information includes also small movements $\Delta\mathbf{x}$ around the nominal position $\mathbf{x}$. In the repository, probabilities $\Pr\left(\triangle s_{t,k} \in \left[\mathrm{v}_{q-1}, \mathrm{v}_q\right] | \mathbf{x}, y_i\right)$ are evaluated numerically by exploiting Monte Carlo simulations for uniformly distributed posture set values $0 \leq \|\Delta\mathbf{x}\| \leq 0.1$ m and $-\pi < \vartheta \leq \pi$. The simulated area size is $d = 1$ m for simulation of body movements, y_1 and $d = 0.25$ m for simulations of body proximity to the UE, y_2 (see the case study in Sect. VI). The path length, namely the distance between the k-th cell tower and the UE is set to $D_k = 500$ m.

The Dirichlet hyperparameter $\boldsymbol{\beta}_{i,k}(q)$ is computed as

$$\boldsymbol{\beta}_{i,k}(q) = \int_{\mathbf{x}\in\mathcal{X}} \Pr\left(\triangle s_{t,k} \in \left[\mathrm{v}_{q-1}, \mathrm{v}_q\right] | \mathbf{x}, y_i\right) d\mathbf{x} \tag{17}$$

and can be replaced in (11) or augment an existing training database.

REFERENCES

[1] X. Lin, J. G. Andrews, A. Ghosh, and R. Ratasuk, "An overview of 3GPP device-to-device proximity services," *IEEE Commun. Mag.*, vol. 52, no. 4, pp. 40–48, Apr. 2014.
[2] M. R. Palattella, "Internet of Things in the 5G era: Enablers, architecture, and business models," *IEEE J. Sel. Areas Commun.*, vol. 34, no. 3, pp. 510–527, Mar. 2016.
[3] *Evolved Universal Terrestrial Radio Access (E-UTRA) and Evolved Universal Terrestrial Radio Access Network (E-UTRAN); Overall Description; Stage 2 (Release 14)*, document 3GPP TS 36 300, Apr. 2018.
[4] R. K. Ganti, F. Ye, and H. Lei, "Mobile crowdsensing: Current state and future challenges," *IEEE Commun. Mag.*, vol. 49, no. 11, pp. 32–39, Nov. 2011.
[5] N. D. Lane, E. Miluzzo, H. Lu, D. Peebles, T. Choudhury, and A. T. Campbell, "A survey of mobile phone sensing," *IEEE Commun. Mag.*, vol. 48, no. 9, pp. 140–150, Sep. 2010.
[6] M. Youssef, M. Mah, and A. Agrawala, "Challenges: Device-free passive localization for wireless environments," in *Proc. 13th Annu. ACM Int. Conf. Mobile Comput. Netw.*, 2007, pp. 222–229.
[7] J. Wilson and N. Patwari, "Radio tomographic imaging with wireless networks," *IEEE Trans. Mobile Comput.*, vol. 9, no. 5, pp. 621–632, May 2010.
[8] S. Savazzi, S. Sigg, M. Nicoli, V. Rampa, S. Kianoush, and U. Spagnolini, "Device-free radio vision for assisted living: Leveraging wireless channel quality information for human sensing," *IEEE Signal Process. Mag.*, vol. 33, no. 2, pp. 45–58, Mar. 2016.
[9] D. Wu, D. Zhang, C. Xu, H. Wang, and X. Li, "Device-free WiFi human sensing: From pattern-based to model-based approaches," *IEEE Commun. Mag.*, vol. 55, no. 10, pp. 91–97, Oct. 2017.
[10] S. Depatla, C. R. Karanam, and Y. Mostofi, "Robotic through-wall imaging: Radio-frequency imaging possibilities with unmanned vehicles," *IEEE Antennas Propag. Mag.*, vol. 59, no. 5, pp. 47–60, Oct. 2017.
[11] S. Shi, S. Sigg, L. Chen, and Y. Ji, "Accurate location tracking from CSI-based passive device-free probabilistic fingerprinting," *IEEE Trans. Veh. Technol.*, vol. 67, no. 6, pp. 5217–5230, Jun. 2018.
[12] B. Guo, Y. J. Chen, N. Lane, Y. Liu, and Z. Yu, "Behavior recognition based on Wi-Fi CSI: Part 1," *IEEE Commun. Mag.*, vol. 55, no. 10, p. 90, Oct. 2017.
[13] B. Guo, Y. J. Chen, N. Lane, Y. Liu, and Z. Yu, "Behavior recognition based on Wi-Fi CSI: Part 2," *IEEE Commun. Mag.*, vol. 56, no. 5, p. 108, May 2018.
[14] *Functions Related to Mobile Station (MS) in Idle Mode and Group Receive Mode (Release 14)*, document 3GPP TS 43 022, Mar. 2017.
[15] K. E. Baddour and N. C. Beaulieu, "Autoregressive modeling for fading channel simulation," *IEEE Trans. Wireless Commun.*, vol. 4, no. 4, pp. 1650–1662, Jul. 2005.
[16] *Technical Specification Group Radio Access Network; Requirements for Support of Radio Resource Management (FDD) (Release 14)*, document 3GPP TS 25.133 V14.2.0, Apr. 2018.
[17] *Universal Mobile Telecommunication System: User Equipment (UE) procedures in Idle Mode and Procedures for Cell Reselection in Connected Mode*, document 3GPP TS 25.304, Nov. 2011.
[18] *Technical Specification Group Radio Access Network; Evolved Universal Terrestrial Radio Access (E-UTRA); Requirements for Support of Radio Resource Management (Release 14)*, document 3GPP TS 36.133 V14.7.0, Apr. 2018.
[19] *Evolved Universal Terrestrial Radio Access (E-UTRA); User Equipment (UE) Procedures in Idle Mode, (Release 8)*, document 3GPP TS 36.304, Jan. 2016.
[20] *AT Command Set for User Equipment (UE) Release 14*, document 3GPP TS 27.007 V14.1.0, Technical Specification 3rd Generation Partnership Project, Sep. 2016.
[21] V. Rampa, G. G. Gentili, S. Savazzi, and M. D'Amico, "EM models for passive body occupancy inference," *IEEE Antennas Wireless Propag. Lett.*, vol. 17, pp. 2517–2520, 2017.
[22] V. Rampa, S. Savazzi, M. Nicoli, and M. D'Amico, "Physical modeling and performance bounds for device-free localization systems," *IEEE Signal Process. Lett.*, vol. 22, no. 11, pp. 1864–1868, Nov. 2015.
[23] V. Konev and S. Vorobeychikov, "Quickest detection of parameter changes in stochastic regression: nonparametric CUSUM," *IEEE Trans. Inf. Theory*, vol. 63, no. 9, pp. 5588–5602, Sep. 2017.
[24] J. Geng, B. Zhang, L. M. Huie, and L. Lai, "Online change detection of linear regression models," in *Proc. IEEE ICASSP*, Shanghai, China, Mar. 2016, pp. 4910–4914.
[25] M. Basseville and I. V. Nikiforov, *Detection of Abrupt Changes: Theory and Application*. Englewood Clifs, NJ, USA: Prentice-Hall, 1993.
[26] H. L. Van Trees, *Detection Estimation and Modulation Theory*, vols. 1–3. New York, NY, USA: Wiley, 2001.
[27] R. E. Madsen, D. Kauchak, and C. Elkan, "Modeling word burstiness using the Dirichlet distribution," in *Proc. 22nd ACM Int. Conf. Mach. Learn. (ICML)*, 2005, pp. 545–552.
[28] M. Abramowitz and I. A. Stegun, *Handbook of Mathematical Functions*, 9th ed. New York, NY, USA: Dover, 1970, ch. 6.

[29] C. Elkan, "Clustering documents with an exponential-family approximation of the Dirichlet compound multinomial distribution," in *Proc. ICML*, 2006, pp. 289–296.
[30] Cellular Data Repository. (2018). *IEEE Dataport*. Accessed: Sep. 5, 2018. [Online]. Available: http://dx.doi.org/10.21227/dqw4-cj02
[31] T. Hastie, S. Rosset, R. Tibshirani, and J. Zhu, "The entire regularization path for the support vector machine," *J. Mach. Learn. Res.*, vol. 5, pp. 1391–1415, Jan. 2004.
[32] E. L. Allwein, R. E. Schapire, and Y. Singer, "Reducing multiclass to binary: A unifying approach for margin classifiers," *J. Mach. Learn. Res.*, vol. 1, pp. 113–141, Sep. 2001.
[33] D. P. Kingma and J. Ba, "Adam: A method for stochastic optimization," in *Proc. 3rd Int. Conf. Learn. Represent. (ICLR)*, San Diego, CA, USA, 2015.
[34] W.-Y. Loh, "Classification and regression trees," *Wiley Interdiscipl. Rev., Data Mining Knowl. Discovery*, vol. 1, no. 1, pp. 14–23, 2011.
[35] M. Spadacini, S. Savazzi, and M. Nicoli, "Wireless home automation networks for indoor surveillance: Technologies and experiments," *EURASIP J. Wireless Commun. Netw.*, vol. 2014, p. 6, Dec. 2014, doi: 10.1186/1687-1499-2014-6.
[36] R. Lutze and K. Waldhör, "Integration of stationary and wearable support services for an actively assisted living of elderly people: Capabilities, achievements, limitations, prospects—A case study," in *Ambient Assisted Living. Advanced Technologies and Societal Change*, W. Reiner and M. Beate, Eds. Cham, Switzerland: Springer, 2017.
[37] J. A. Fuemmeler, G. K. Atia, and V. V. Veeravalli, "Sleep control for tracking in sensor networks," *IEEE Trans. Signal Process.*, vol. 59, no. 9, pp. 4354–4366, Sep. 2011.
[38] A. Montanari, S. Nawaz, C. Mascolo, and K. Sailer, "A study of Bluetooth low energy performance for human proximity detection in the workplace," in *Proc. IEEE PerCom*, Kona, HI, USA, Mar. 2017, pp. 90–99.
[39] A. Nahapetian, "Side-channel attacks on mobile and wearable systems," in *Proc. 13th IEEE CCNC*, Las Vegas, NV, USA, Jan. 2016, pp. 243–247.
[40] A. J. Aviv, K. Gibson, E. Mossop, M. Blaze, and J. M. Smith, "Smudge attacks on smartphone touch screens," in *Proc. 4th USENIX Conf. Technol. (WOOT)*. Berkeley, CA, USA: USENIX Association, 2010, pp. 1–7.
[41] L. Rokach, "Taxonomy for characterizing ensemble methods in classification tasks: A review and annotated bibliography," *Comput. Statist. Data Anal.*, vol. 53, no. 12, pp. 4046–4072, 2009.

STEFANO SAVAZZI received the M.Sc. degree (Hons.) in telecommunication engineering and the Ph.D. degree (Hons.) in information technology from Politecnico di Milano, Italy, in 2004 and 2008, respectively. He was a Visiting Researcher with Uppsala University in 2005, the University of California at San Diego in 2007, and Forschungszentrum Telekommunikation, Wien, in 2010. In 2012, he joined the Consiglio Nazionale delle Ricerche, Institute of Electronics, Computer and Telecommunication Engineering, Italy, as a Researcher. His current research interests include signal processing, machine learning and networking design aspects for the Internet of Things, and cooperative and cognitive sensor networks for radio vision and localization. He received the Dimitris N. Chorafas Foundation Award for the Best Ph.D. dissertation.

SANAZ KIANOUSH received the M.Sc. degree from the Islamic Azad University of Tehran, Iran, in 2008, and the Ph.D. degree in electronic engineering from the University of Pavia, Italy, in 2014. From 2008 to 2010, she was a Lecturer with Islamic Azad University Sary, Iran. She has been holding post-doctoral position at the Consiglio Nazionale delle Ricerche, Wireless Communication Systems Group, Institute of Electronic Informatics and Telecommunication Engineering, since 2014. Her research interests include statistical signal processing in communication systems, design and develop algorithms for device free radio-based localization, and human activity recognition for assisted living in wireless networks.

VITTORIO RAMPA received the degree (Hons.) in electronics engineering from Politecnico di Milano in 1984. In 1986, he joined the Consiglio Nazionale delle Ricerche (CNR) of Italy as a Researcher. From 1999 to 2014, he was an Adjunct Professor with Politecnico di Milano, where he taught courses on software-defined radios and radio localization systems. In 2001, he became a Senior Researcher with the Institute of Electronics, Computer and Telecommunication Engineering. His main research interests include signal processing algorithms and architectures for wireless communications, radio vision algorithms and systems, virtual instrumentation techniques for test and verification of wireless systems.

UMBERTO SPAGNOLINI has been a Faculty Member with Politecnico di Milano since 1990, where he is currently Professor of statistical signal processing. He has authored the book *Statistical Signal Processing in Engineering* (J. Wiley, 2017). His research in statistical signal processing covers remote sensing and communication systems with over 300 papers on peer-reviewed journals/conferences and patents. His specific areas of interest include channel estimation and space-time processing for single/multi-user wireless communication systems, co-operative and distributed inference methods, parameter estimation/tracking, and wavefield interpolation for remote sensing (UWB radar and oil exploration). He was recipient/co-recipient of the Best Paper Awards from EAGE on geophysical signal processing methods in 1991 and 1998, the IEEE ICASSP 2006 on array processing, and SPAWC 2007 and WRECOM 2007 on distributed synchronization for wireless sensor networks. He served as a part of the IEEE editorial boards and a member of the technical program committees of several conferences for all areas in his research interests.